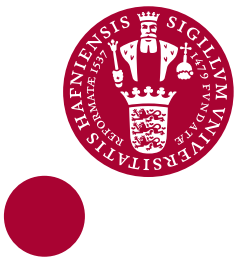

A visual rating scale for cingulate island sign on 18F-FDG-PET to differentiate dementia with Lewy bodies and Alzheimer's disease

Gjerum, Le; Frederiksen, Kristian Steen; Henriksen, Otto Mølby; Law, Ian; Anderberg, Lasse; Andersen, Birgitte Bo; Bjerregaard, Eva; Hejl, Anne Mette; Høgh, Peter; Hasselbalch, Steen Gregers

Published in:
Journal of the Neurological Sciences

DOI:
10.1016/j.jns.2019.116645

Publication date:
2020

Document version
Publisher's PDF, also known as Version of record

Journal of the Neurological Sciences 410 (2020) 116645

Contents lists available at ScienceDirect

Journal of the Neurological Sciences

journal homepage: www.elsevier.com/locate/jns

A visual rating scale for cingulate island sign on 18F-FDG-PET to differentiate dementia with Lewy bodies and Alzheimer's disease

Le Gjerum[a,*], Kristian Steen Frederiksen[a], Otto Mølby Henriksen[b], Ian Law[b], Lasse Anderberg[b], Birgitte Bo Andersen[a], Eva Bjerregaard[a], Anne-Mette Hejl[c], Peter Høgh[d,e], Steen Gregers Hasselbalch[a]

[a] Department of Neurology, Danish Dementia Research Centre, Rigshospitalet, University of Copenhagen, Blegdamsvej 9, DK-2100 Copenhagen, Denmark
[b] Department of Clinical Physiology, Nuclear Medicine & PET, Rigshospitalet, University of Copenhagen, Blegdamsvej 9, DK-2100 Copenhagen, Denmark
[c] Department of Neurology, Bispebjerg Hospital, University of Copenhagen, Bispebjerg Bakke 23, DK-2400 Copenhagen, Denmark
[d] Regional Dementia Research Center, Department of Neurology, Zealand University Hospital, Sygehusvej 10, DK-4000 Roskilde, Denmark
[e] Department of Clinical Medicine, University of Copenhagen, Blegdamsvej 3B, DK-2200 Copenhagen, Denmark

ARTICLE INFO

Keywords:
Cingulate island sign
FDG-PET
Dementia with Lewy bodies
Alzheimer's disease
Dual pathology
Visual rating scale

ABSTRACT

Valid diagnosis of dementia with Lewy bodies (DLB) is essential to establish appropriate treatment and care. However, the diagnostic accuracy is complicated by clinical and pathological overlap with Alzheimer's disease (AD). Cingulate island sign (CIS), defined as sparing of posterior cingulate cortex (PCC) relative to precuneus and cuneus on 18F-fluoro-deoxy-glucose positron emission tomography (18F-FDG-PET), is included in the revised diagnostic DLB criteria. There are no guidelines for the visual grading of CIS, although visual rating is a fast-applicable method in a clinical setting.

The objective was to develop a robust visual CIS scale and evaluate the performance in differentiating DLB with and without amyloid beta pathology (Aβ+/−), and AD.

18F-FDG-PET scans from 35 DLB patients, 36 AD patients, and 23 healthy controls were rated according to a visual CIS scale based on specific reading criteria. The visual CIS scale was validated against a quantitative CIS ratio derived from a region of interest analysis of PCC, precuneus, and cuneus.

DLB patients had a significantly higher visual CIS score compared to AD patients, and controls.

A cut-off visual CIS score of 4 significantly differentiated DLB Aβ− patients from DLB Aβ+ patients.

In conclusion, the visual CIS scale is clinically useful to differentiate DLB from AD. The degree of CIS may be related to Aβ pathology in DLB patients.

1. Introduction

Dementia with Lewy bodies (DLB), which is pathologically characterized by accumulation of Lewy bodies (LB), is the second most common cause of neurodegenerative dementia after Alzheimer's disease (AD) [24]. Early and accurate diagnosis of DLB is essential to enable appropriate treatment and care, in addition to identify and manage clinical features including motor and psychiatric symptoms, severe autonomic dysfunction and hazardous antipsychotic sensitivity [26]. A valid diagnosis is also central for predicting the prognosis of the disease and planning clinical trials, but the diagnostic process may be complicated by substantial overlap in clinical and neuropsychological features between AD and DLB [23]. Furthermore, the frequent occurrence of pathological heterogeneity in DLB patients, particularly coexisting AD pathology, i.e. amyloid beta (Aβ) plaques and tau tangles, can contribute to diverse clinical presentations [33,34]. Aβ pathology in patients with DLB has been associated with faster cognitive decline and shorter survival compared to the DLB patients with pure LB pathology

Abbreviations: Aβ, amyloid beta; AD, Alzheimer's disease; AUC, area under the curve; CI, confidence interval; CIS, cingulate island sign; CSF, cerebrospinal fluid; CT, computed tomography; DAT, dopamine transporter; DLB, dementia with Lewy bodies; LB, Lewy bodies; MMSE, mini mental state examination; MRI, magnetic resonance imaging; PCC, posterior cingulate cortex; PET, positron emission tomography; ROI, region of interest; SPECT, single photon emission computed tomography; SUV, standardized uptake value; 11C-PiB, 11C-Pittsburgh compound B; 123I-FP-CIT, 123I-2β-carbomethoxy-3β-(4-iodophenyl)-N-(3-fluoropropyl)-nortropane; 18F-FDG, 18F-fluoro-deoxy-glucose

* Corresponding author.
E-mail addresses: le.gjerum@regionh.dk (L. Gjerum), steen.gregers.hasselbalch@regionh.dk (S.G. Hasselbalch).

https://doi.org/10.1016/j.jns.2019.116645
Received 15 October 2019; Received in revised form 17 December 2019; Accepted 21 December 2019
Available online 24 December 2019

[6,16]. These findings underline the clinical relevance of identifying coexisting Aβ pathology in DLB patients.

Functional neuroimaging has become a commonly used supplement to the clinical diagnosis of dementia [36], and has also been introduced in the diagnostic criteria for both DLB and AD [26,27]. Several studies have demonstrated occipital hypometabolism as a supportive feature to distinguish DLB patients from AD patients on positron emission tomography (PET) imaging using 18F-fluoro-deoxy-glucose as tracer (18F-FDG-PET) [1,18,19,29].

Cingulate island sign (CIS) is another identified feature on 18F-FDG-PET to support the diagnosis of DLB, and has been found to be more specific than occipital hypometabolism for DLB [21]. CIS is defined as preserved metabolism of the posterior cingulate cortex (PCC) relative to reduced metabolism in the precuneus and the cuneus, and is included in the updated diagnostic DLB criteria [26]. The CIS ratio, defined as the measure of FDG uptake in the PCC divided by the sum of the uptake in the precuneus and the cuneus, is higher in DLB patients compared to AD patients as demonstrated by a semi-quantitative method [11,15,19,21,31]. A quantitative method can be time consuming, requires standardized acquisition and analysis of both the 18F-FDG-PET and the structural scan, i.e. either computed tomography (CT) or magnetic resonance imaging (MRI), and the specific software may only be accessible in expert centres. Of interest, a dichotomous visual interpretation of CIS (present or absent) had a higher diagnostic accuracy compared to the quantitative CIS ratio in distinguishing DLB patients from AD patients [21]. However, there are no established visual criteria for the degree of CIS, even though visual rating of other imaging biomarkers and modalities are commonly used and has proven to be a fast, reliable and reproducible method in clinical practice [14,36,37]. The application of a standardized method to classify and interpret the presence of CIS may enhance the utilization of relevant diagnostic information, along with improving the diagnostic accuracy of DLB. Furthermore, a visual rating scale can easily be implemented into the clinical practice across centres and assist the less experienced nuclear medicine physicians.

The objectives of this study were (1) to develop a robust visual rating scale for the presence of CIS on 18F-FDG-PET (the visual CIS scale); (2) to evaluate the reproducibility and the accuracy of the visual CIS scale to differentiate DLB patients and AD patients; (3) to compare the performance of the visual CIS scale to a quantitative method for CIS (the quantitative CIS ratio) and 18F-FDG-PET visual features of occipital involvement and forced diagnosis; (4) to examine whether coexisting Aβ pathology influenced the presence of CIS for the DLB patients.

2. Materials and methods

2.1. AD and DLB study population

The study population consisted of retrospectively identified patients with a clinical diagnosis of DLB according to the DLB criteria [25] and AD according to the AD criteria [27] diagnosed from 2011 to 2017 at four Danish memory clinics in the greater Copenhagen area (Rigshospitalet, Glostrup Hospital, Bispebjerg Hospital, and Roskilde Hospital).

The dementia diagnoses were confirmed according to the established clinical criteria by an experienced dementia specialist (SGH, AH, or PH) based on patient files from baseline to the most recent clinical follow up and all available examination results (except the 18F-FDG-PET findings).

All eligible patients had a structural scan, i.e. either CT or MRI, a 18F-FDG-PET scan, and determination of the brain Aβ status, i.e. either measurement of Aβ 1–42 (Aβ42) in the cerebrospinal fluid (CSF) or PET imaging using the ligand 11C-Pittsburgh compound B (11C-PiB-PET).

For patients with DLB an abnormal 123I-2β-carbomethoxy-3β-(4-iodophenyl)-N-(3-fluoropropyl)-nortropane (123I-FP-CIT) dopamine transporter single photon emission computed tomography (123I-FP-CIT-DAT-SPECT) scan was also required.

Thirty-seven patients with a clinical diagnosis of DLB and 37 patients with a clinical diagnosis of AD matched on age, sex, and MMSE were included.

The retrospective use of clinical data was approved by the Danish Patient Safety Authority (no. 3-3013-2703/1).

2.2. Healthy controls

A group of 23 healthy elderly controls aged over 60 years with normal MRI and 18F-FDG-PET results, and normal neuropsychology scores from the Memory Clinic at Rigshospitalet was also included. The controls consisted of 18 healthy research volunteers and five subjects with subjective cognitive decline in whom dementia and neurodegenerative disease had been ruled out. All controls had no evidence of brain amyloid accumulation, i.e. normal concentration of Aβ42 in CSF, except three of the healthy research volunteers who did not undergo assessment of brain amyloid.

All healthy research volunteers gave a written informed consent, and the inclusion was approved by the Danish National Committee on Health Research (no. H-1-2014-126).

2.3. Clinical examinations

All patients and controls underwent a standardized diagnostic dementia assessment including medical history, physical and neurological examinations, cognitive testing (i.e. Mini mental state examination (MMSE) and Addenbrooke's cognitive examination), routine blood screening, and a structural scan, i.e. either CT or MRI.

The dementia patients were followed up longitudinally as part of the standard clinical routine, and 93% of the patients were followed for at least 12 months.

2.4. Assessment of brain amyloid

The brain amyloid accumulation was determined by either Aβ42 in CSF (n = 76), 11C-PiB-PET imaging (n = 5), or both (n = 10). If the Aβ biomarkers were incongruent (n = 5) the result of the 11C-PiB-PET image determined the Aβ status.

The CSF was collected by lumbar puncture in polypropylene tubes, and Aβ42 was analysed with the enzyme-linked immunosorbent assay (ELISA) using the commercially available kit (Innotest, Fujirebio, Europe, Ghent, Belgium). An abnormal Aβ42 (< 550 pg/mL) was indicated as Aβ+, whereas a normal Aβ42 was indicated as Aβ− [40].

2.5. Imaging

Imaging was performed over a seven-year period at different hospitals using a range of scanner systems. General aspects of MRI, 123I-FP-CIT-DAT-SPECT, 11C-PiB-PET, and 18F-FDG-PET imaging are summarized in subsection 2.5.1–2.5.5. Imaging details are provided in Appendix A.

2.5.1. Acquisition of MRI

MRI was performed on a clinical 1.5 or 3.0 Tesla system. A high-resolution 3D T1 weighted MRI sequence suitable for tissue segmentation was available in 77 subjects. A semi-quantitative CIS ratio analysis of the high-resolution 3D T1 weighted MRI sequence was performed as describe in subsection 2.5.5.1.

2.5.2. Analysis of 123I-FP-CIT-DAT-SPECT

A visual interpretation of reduced symmetric or asymmetric tracer uptake in putamen and/or caudate nucleus was defined as abnormal, supported by the semiquantitative analysis of the specific binding ratio of striatum, caudate nucleus, and putamen relative to occipital cortex and the putamen/caudate nucleus uptake ratio [5,22].

2.5.3. Analysis of 11C-PiB-PET

A visual interpretation of increased tracer uptake in at least two cortical AD specific regions at the level of or above white matter supported by cortex-to-cerebellar grey matter uptake ratio > 1.5 was defined as abnormal [28]. An abnormal 11C-PiB-PET was indicated as Aβ+, whereas a normal 11C-PiB-PET was indicated as Aβ− .

2.5.4. Acquisition of 18F-FDG-PET

The PET imaging was performed according to the international practice guideline [35]. PET images were acquired using clinical PET/CT or PET/MRI systems after an intravenous bolus of 200–300 MBq 18F-FDG as a 10 min static scan during the 40–60 min post-injection time window. All images were reconstructed using CT based attenuation correction [2].

2.5.5. Analysis of 18F-FDG-PET

2.5.5.1. Analysis of quantitative CIS ratio. The high-resolution 3D T1 weighted MRI sequence was segmented using FreeSurfer (version 5.3.0) [8] to generate region of interests (ROIs) of PCC, precuneus, cuneus, and cerebellar grey matter for each hemisphere based on the Desikan-Killiany Atlas. The 18F-FDG-PET image of each patient was fused to the segmented MRI and the mean ROI values were obtained. Only non-partial volume corrected PET data was used, as partial volume corrected by the Symmetric Geometric Transfer Matrix method [12] was not Please insert hyphen: "suf- < br > ficiently"sufficiently robust. The mean standardized uptake value (SUV) of each region was normalized to cerebellum. In each hemisphere the ratio for the mean SUV in the PCC ROI was divided by the mean SUV in the combined precuneus plus cuneus ROIs, the quantitative CIS ratio was derived by averaging the ratios for each hemisphere [21].

2.5.5.2. Standardized reading approach for the visual interpretation. A clinical standardized reading approach in SyngoVia (SyngoVia, MI Neurology, Siemens Healthcare, Erlangen, Germany) of the 18F-FDG-PET scan co-registered to the structural scan (i.e. low-dose CT, non-enhanced diagnostic CT or MRI) was performed.

The visual interpretation of the 18F-FDG-PET scan was performed in the following order: First, scoring of the visual CIS scale, then rating of occipital hypometabolism, and finally assessment of the forced diagnosis. Rating of CIS was based on visual evaluation only, whereas evaluation of occipital hypometabolism and forced diagnosis was supported by the statistical surface projections from a normal database supplied by the software vendor (age 46–75 years) using cerebellum as a reference region.

Two experienced nuclear medicine physicians (IL and OMH) blinded to all clinical data visually assessed all the 18F-FDG-PET scans. In case of disagreement a consensus evaluation was performed between the two readers.

2.5.5.3. Development of the visual CIS-scale. To define the degree of CIS for the visual scale, we evaluated 18F-FDG-PET images from five DLB patients and ten AD patients with a wide range of CIS presentations. Based on the evaluations of the 18F-FDG-PET images, the visual CIS scale was developed and adjusted to the final version by two experienced nuclear medicine physicians (IL and OMH).

2.5.5.4. Standardized reading approach for the visual CIS-scale. A standard reading approach was used to standardize the 18F-FDG-PET images and optimize the visualization of the CIS region (Fig. 1):

- the 18F-FDG-PET scan was displayed on a clinical workstation using SyngoVia with the PET image superimposed on the structural scan.
- the scan was displayed in “PET Rainbow” and windowing adjusted to basal ganglia red and cerebellum green/yellow with red hues.
- three-way orthogonal view approximately along AC-PC plane with both sagittal and axial planes through PCC, precuneus, and cuneus.

The visual CIS scoring was based on both sagittal and axial views.

2.5.5.5. Scoring of the visual CIS scale. First, the degree of hypometabolism in PCC, precuneus, and cuneus was classified for each hemisphere as “none”, “mild”, or “moderate-to-severe”.

Secondly, the presence of CIS was based on the degree of hypometabolism in PCC, precuneus, and cuneus together with a visual, interpretation of CIS including influence of central or cortical atrophy, and rated for each hemisphere according to the following criteria:

0 = absent (PCC similar or lower than precuneus and cuneus).
1 = intermediate (e.g. PCC hypometabolic, but less than precuneus and cuneus, or only precuneus lower than PCC).
2 = present (typically PCC normal and both precuneus and cuneus lower).

If the activity uptake in precuneus or cuneus was considered reduced because of adjacent leukoaraiosis or ischemia on the available structural scan the rating was changed to 0.

Finally, the ratings from each hemisphere were summed to a visual CIS score. Three examples of scorings of the visual CIS scale are giving in Fig. 2.

For clinical operationalization the visual CIS score was classified as:

Score 0 = “no CIS”.
Score 1–2 = “possible CIS”.
Score 3–4 = “definite CIS”.

2.5.5.6. Occipital hypometabolism. Occipital hypometabolism was assessed in lateral and medial occipital cortices and rated as “present” or “absent”.

2.5.5.7. Forced diagnosis. This approach was adopted to mimic the usual reading approach of a nuclear medicine physician. The forced diagnosis was based on the overall visual interpretation of the 18F-FDG-PET scan including typical features of DLB (predominant occipital involvement with no or minimal involvement of frontal or anterior temporal cortex) and typical features of AD (anterior temporal, mesial temporal, or AD like parietotemporal hypometabolism with occipital sparing). The readers were asked to give a forced diagnosis of the most likely aetiology (“DLB”, “AD”, “other abnormal”, or “normal”).

2.6. Statistical analysis

Differences between groups were assessed with Kruskal-Wallis tests followed by Mann-Whitney post-hoc tests or one-way ANOVA tests followed by Tukey post-hoc tests for continuous variables, and Pearson's or Fischer's Chi-square test for count variables, where appropriate.

The interrater agreement was quantified by Cohen's weighted Kappa. The Spearman's correlation analysis was applied for comparing the quantitative CIS ratio values and the visual CIS scores, and for verifying the correlations between visual CIS score, MMSE score, age, education, and symptom duration for all subjects and DLB patients. For the latter, the Spearman correlation results were corrected by false discovery rate (FDR) correction. The diagnostic accuracy for each binary disease group comparison was reported as sensitivity, specificity, balanced accuracy, and area under the receiver-operator characteristic curve (AUC). Balanced accuracy is defined as the average of sensitivity and specificity for the cut-off score, and compensates for the imbalanced number in the disease groups [4].

The optimal cut-off was established by maximizing the Youden index. Youden index is defined as the sum of sensitivity and specificity minus one [39].

Statistical analysis was performed using SAS Studio software, version 9.4 (SAS Institute Inc., Cary, NC, USA) and GraphPad Prism 8.0.0

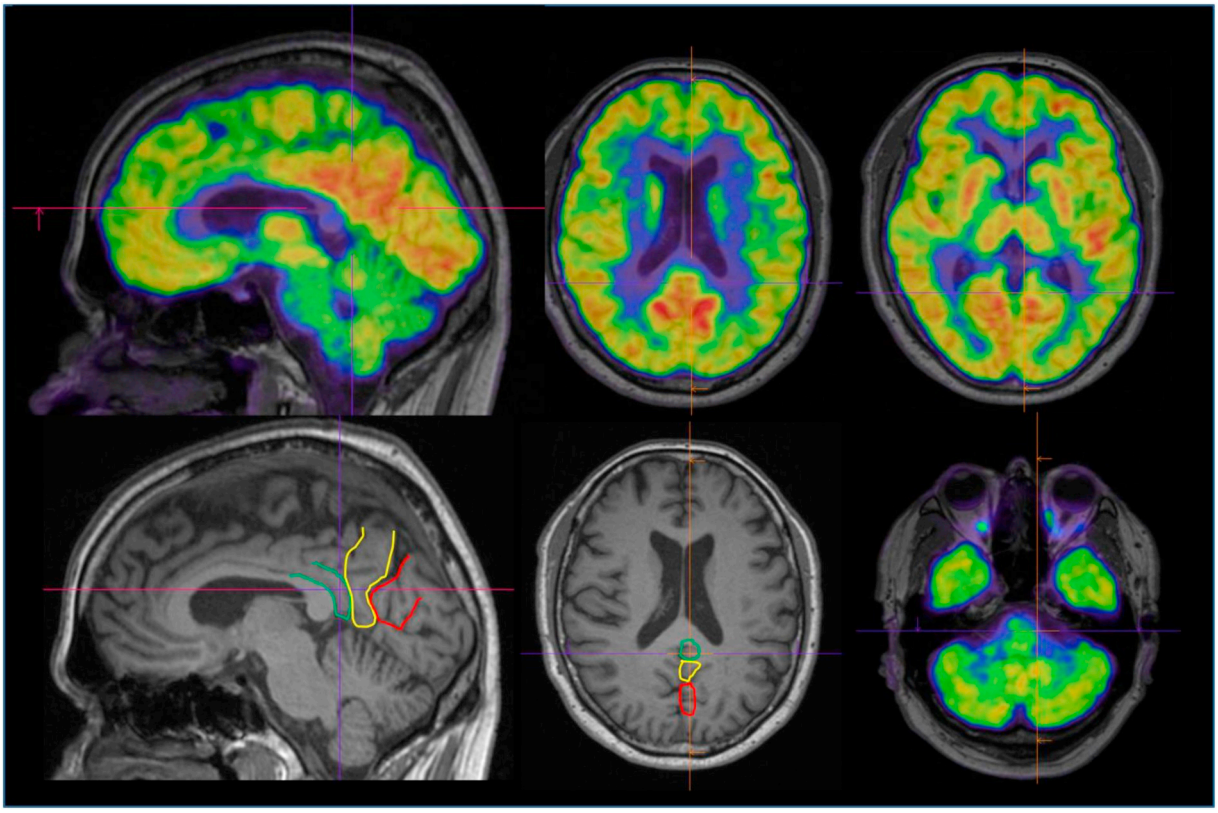

Fig. 1. Standardized reading approach of 18F-FDG-PET.
Abbreviations: MRI = magnetic resonance imaging; PCC = posterior cingulate cortex; 18F-FDG-PET = 18F-fluoro-deoxy-glucose positron emission tomography; MRI and 18F-FDG-PET image displayed in saggital and axial plane in Scenium with orientation through PCC (green), precuneus (yellow) and cuneus (red).

for Windows (GraphPad Software, San Diego, California USA). A two-sided *p*-value < .05 was considered indicative of statistical significance.

3. Results

3.1. Baseline characteristics

Two patients with a clinical diagnosis of DLB and one patient with a clinical diagnosis of AD were excluded during the visual assessment of the 18F-FDG-PET scans due to poor quality. The flow diagram of the study population is shown in (Appendix B, Fig. B.1). Demographics are shown in Table 1. There were no significant differences in the baseline demographics between the two dementia groups (DLB patients and AD patients) or the DLB subgroups (DLB Aβ− patients and DLB Aβ+ patients). The controls had a significantly higher MMSE score than all dementia groups (AD, DLB Aβ− patients and DLB Aβ+ patients) and

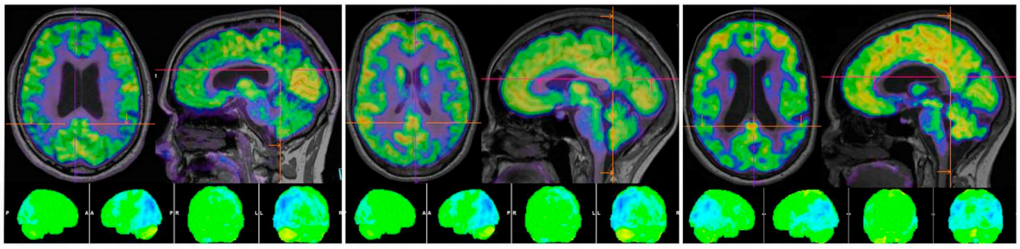

		71-years old male diagnosed with AD with MMSE-score 25 and a positive Aβ-biomarker	66-years old female diagnosed with DLB with MMSE-score 29 and a positive Aβ-biomarker	75-years old female diagnosed with DLB with MMSE-score 29 and a negative Aβ-biomarker
Degree of hypometabolism (R/L)	PCC	moderate-to-severe/mild	none/mild	none/none
	Precuneus	moderate-to-severe/mild	none/mild	moderate-to-severe/moderate-to-severe
	Cuneus	none/none	none/moderate-to-severe	moderate-to-severe/moderate-to-severe
Visual CIS score (R+L)		0 (0+0)	1 (0+1)	4 (2+2)
Classification of CIS		No CIS	Possible CIS	Definite CIS
Quantitative CIS ratio		0.95	1.17	1.16

Fig. 2. 18F-FDG-PET images with examples of the visual CIS-score and quantitative CIS ratio.
Abbreviations: Aβ = amyloid beta; AD = Alzheimer's disease; CIS = cingulate island sign; DLB = dementia with Lewy bodies; L = left; MMSE = Mini-Mental State Examination; PCC = posterior cingulate cortex; R = right; 18F-FDG-PET = 18F-fluoro-deoxy-glucose positron emission tomography; Axial and sagittal view of the PET image superimposed on the high-resolution 3D T1 weighted MRI sequence (top) and the statistical surface (right lateral, left lateral, anterior, and posterior view) projections using cerebellum as a reference region compared to a healthy age-matched control group (bottom).

Table 1
Baseline demographics.

	AD	Controls	DLB	DLB Aβ−	DLB Aβ+
Subjects, n	36	23	35	19	16
Female, n (%)	11 (30.6%)	8 (34.8%)	10 (28.6%)	4 (21.0%)	6 (37.5%)
Age, mean years ± SD	70.6 ± 6.3	68.7 ± 6.1	69.9 ± 6.8	68.0 ± 8.3	72.1 ± 3.5*
MMSE, mean score ± SD	25.8 ± 2.9*	29.3 ± 1.2	26.3 ± 3.2*	26.1 ± 3.3*	26.6 ± 3.1*
Education, mean years ± SD	13.5 ± 2.8	14.5 ± 2.4	12.8 ± 2.8*	13.0 ± 2.7	12.6 ± 3.0
Symptom duration, mean years ± SD	3.1 ± 3.1	NA	2.9 ± 2.8	2.3 ± 2.2	3.6 ± 3.4

Abbreviations: Aβ = amyloid beta; AD = Alzheimer's disease; DLB = dementia with Lewy bodies; MMSE = Mini-Mental State Examination; n = number; NA = not applicable; SD = standard deviation;
* Differ significantly from Controls ($p < .05$).

longer education in years compared to DLB patients.

3.2. Reliability of the visual CIS scale

According to Cohen's weighted kappa, the interrater agreement of the visual CIS score between the two readers was 0.73 (95% CI 0.63;0.83). The two readers had disagreement of the visual CIS scores in 26 of 97 cases, of which 61% was of one grade, 35% was of two grades, 4% (1 case) was of three grades. The distribution of the visual CIS scores between the two readers are shown in Appendix C, Table C.1.

The quantitative CIS ratio analysis was performed in the 77 subjects with a high-resolution 3D T1 weighted MRI sequence. The correlation of the visual CIS score with the quantitative CIS ratio value was moderate-to-strong (Spearman's correlation coefficient, $r = 0.60$, 95% CI 0.44–0.73; $p < .0001$) (Fig. 3).

3.3. DLB patients and AD patients

Table 2 shows that the median visual CIS score was significantly higher for DLB patients in comparison to AD patients, and controls. In line with this, the mean quantitative CIS ratio was significantly higher for DLB patients compared to AD patients and controls. Most of the AD patients (75%) and controls (87%) were evaluated to have “no CIS” based on the classification of the visual CIS score in comparison to a minority of the DLB patients (26%).

An optimal cut-off score on the visual CIS scale of ≥2 had a sensitivity of 51% and a specificity of 92% in differentiating DLB patients and AD patients, yielding a balanced accuracy of 72% (Table 3). In comparison, the optimal cut-off value of ≥0.98 on the quantitative CIS ratio separated DLB patients and AD patients with a higher sensitivity of 88% and a lower specificity of 67%, yielding a balanced accuracy of 77%. When comparing the performance of the two methods by an AUC analysis, we observed no significant difference ($p = .45$) in differentiating DLB patients and AD patients, although the latter method had a slightly better performance. Also, the visual CIS scale did not differ in performance when compared with visual interpretation of occipital hypometabolism and forced diagnosis for distinguishing DLB patients and AD patients (Table 3).

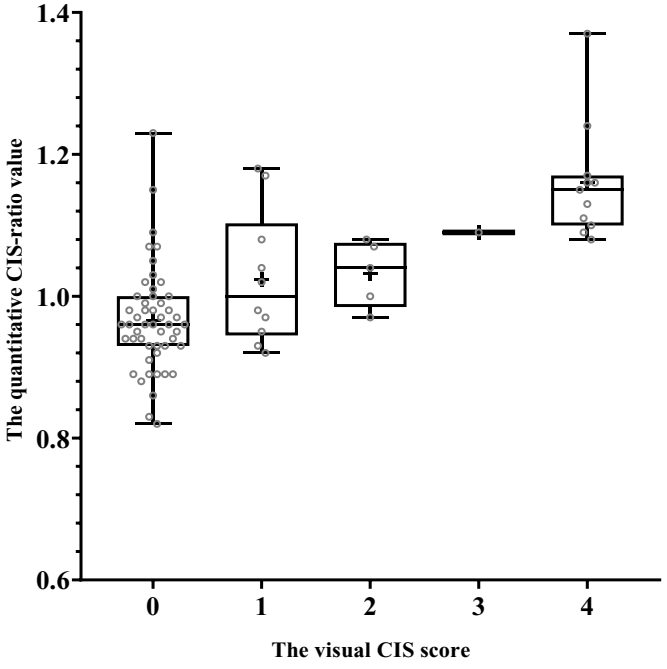

Fig. 3. Correlation of the visual CIS score and the quantitative CIS ratio value. Abbreviations: CIS = cingulate island sign; Boxplot graph with the boxes corresponding to median values with indications of the 25th and 75th percentiles, and the whiskers show the minimum and maximum values. The + indicates the mean. All the subjects are plotted as ○. The Spearman's correlation coefficient of all five groups on the visual CIS score (0, 1, 2, 3, and 4) and the quantitative CIS ratio was $r = 0.60$ (95% CI 0.44–0.73, $p < .0001$).

3.4. Amyloid positive and amyloid negative DLB patients

The DLB Aβ− patients had the highest median visual CIS score of 4, followed by DLB Aβ+ patients with a median score of 1, and lastly the AD patients with a median score of 0. However, the visual CIS score were only significant different between the AD patients and the DLB subgroups, although the difference between DLB Aβ+ patients and DLB Aβ− patients reached a trend level of $p = .06$. A significant larger proportion of the DLB Aβ− patients (58%) was classified with “definite CIS”, when compared both to DLB Aβ+ patients (25%) and to AD patients (3%) (Table 2).

As shown in Table 3, an optimal cut-off score of 4 on the visual CIS scale distinguish DLB Aβ− patients from the DLB Aβ+ patients and AD patients with a balanced accuracy of 70% and 80% respectively. When applying the Fishers exact test, the proportion of DLB Aβ− patients with a visual CIS score 4 was significantly higher compared to the DLB Aβ+ patients and AD patients. Whereas, the proportion of DLB Aβ+ patients with an optimal cut-off score ≥1 was significantly higher than the AD patients.

No significant differences were observed between the visual CIS scale and the quantitative CIS ratio for separating the diagnostic groups.

3.5. Clinical correlations

Box plot of MMSE scores across CIS scores (Appendix D, Fig. D.1) and Kruskal-Wallis test ($p = .55$) did not indicate an association of MMSE with visual CIS score.

Furthermore, the pairwise correlations between the visual CIS score and MMSE score, age, education, and symptom duration for all subjects and DLB patients were investigated with a Spearman correlation analysis both for all subjects and for DLB patients (Appendix D, Table D.1 and D.2). The visual CIS score was not significant correlated with any clinical variable, neither for all subjects or for DLB patients.

Table 2
The visual CIS scale and the quantitative CIS ratio.

	AD	Controls	DLB	DLB Aβ−	DLB Aβ+
Subjects, n	36	23	35	19	16
Visual CIS score					
0/1/2/3/4, n	27/6/2/0/1	20/1/2/0/0	12/5/3/1/14	5/2/0/1/11	7/3/2/1/3
Median score (IQR)	0 (0.5)	0 (0)	2 (4)*	4 (4)*,‡	1 (2.5)*
Visual CIS classification					
No CIS/Possible CIS/Definite CIS, n	27/8/1	20/3/0	12/8/15*	5/3/11*	7/5/4*
Quantitative CIS ratio					
Mean value ± SD	0.98 ± 0.08	0.96 ± 0.07	1.09 ± 0.10*	1.11 ± 0.10*	1.05 ± 0.09

Abbreviations: Aβ = amyloid beta; AD = Alzheimer's disease; CIS = cingulate island sign; DLB = dementia with Lewy bodies; IQR = interquartile range; n = number; SD = standard deviation;
* Differ significantly from AD and controls ($p < .05$).
‡ Trend difference from DLB Aβ + ($p = .06$).

Table 3
Diagnostic accuracy of the visual CIS scale, quantitative CIS ratio and 18F-FDG-PET visual features.

	DLB versus AD			
	Sens.	Spec.	Bal. acc.	AUC (95% CI)
Visual CIS score ≥2	51.4%	91.7%	71.6%	0.77 (0.64–0.89)
Quantitative CIS ratio value ≥0.98	87.5%	66.7%	77.1%	0.82 (0.70–0.94)
Occipital hypometabolism	54.3%	91.7%	73.0%	0.74 (0.63–0.85)
Forced diagnosis	51.4%	94.4%	72.9%	0.78 (0.66–0.90)
	DLB Aβ− versus AD			
	Sens.	Spec.	Bal. acc.	AUC (95% CI)
Visual CIS score = 4	63.2%	97.2%	80.2%	0.85 (0.71–0.99)
Quantitative CIS ratio value ≥1.04	85.7%	86.7%	86.2%	0.88 (0.77–0.98)
	DLB Aβ+ versus AD			
	Sens.	Spec.	Bal. acc.	AUC (95% CI)
Visual CIS score ≥1	56.3%	75.0%	65.6%	0.65 (0.45–0.85)
Quantitative CIS ratio value ≥0.99	80.0%	76.7%	78.3%	0.74 (0.54–0.94)
	DLB Aβ− versus DLB Aβ+			
	Sens.	Spec.	Bal. acc.	AUC (95% CI)
Visual CIS score = 4	57.9%	81.3%	69.6%	0.73 (0.52–0.93)
Quantitative CIS ratio value ≥1.04	85.7%	50.0%	67.9%	0.66 (0.43–0.90)

Abbreviations: Aβ = amyloid beta; AD = Alzheimer's disease; AUC = the area under the receiver operating characteristic curve; Bal. acc. = balanced accuracy; CI = confidence interval; CIS = cingulate island sign; DLB = dementia with Lewy bodies; Sens. = sensitivity; Spec. = specificity; 18F-FDG-PET = 18F-fluoro-deoxy-glucose positron emission tomography.

4. Discussion

CIS is a supportive marker of DLB on 18F-FDG-PET, and is useful in the discrimination of DLB from AD [26], however, a visual rating scale for CIS has been lacking. With this study we aimed to develop a robust visual rating scale from clinically acquired 18F-FDG-PET scans to detect the degree of CIS. We found an acceptable interrater agreement with most disagreements amounting to a single grade in the low-grade group, and a moderate-to-strong correlation with the quantitative CIS ratio, suggesting that the visual CIS scale is useful in a clinical setting as an aid in assessment of CIS.

Furthermore, we found significant differences between the groups median visual CIS scores in both the diagnostic groups analysis (DLB, AD, and controls) and the subgroups analysis (DLB Aβ−, DLB Aβ+, and AD). Notably, a cut-off visual CIS score of 4 could significantly differentiate the DLB Aβ− patients from the DLB Aβ+ patients, which reflects that the degree of CIS may be associated with Aβ pathology in DLB patients.

The original study introducing visual interpretation of CIS for differentiating DLB from AD by Lim et al. found CIS to be highly specific for DLB with a specificity of 100% and a sensitivity ranging from 62% to 86% [21]. The higher diagnostic accuracy in the prior study compared to our findings may be due to a restricted dichotomized rating of CIS in a relatively small study cohort of 14 DLB patients and 10 AD patients, together with only 29% of DLB patients having AD pathology. In contrast, we aimed to characterize the degree of CIS in the pathological heterogenous DLB patients considering previous studies have demonstrated higher CIS ratio in DLB patients compared to AD patients [11,15,19,21,31] together with over half of pathologically confirmed DLB cases have coexisting AD pathology [3,10].

We evaluated the performance of the visual CIS scale against a quantitative CIS method as the presence of CIS has mainly been demonstrated by various quantitative methods [11,15,19,21,31,38]. In accordance with the previous studies, we found a significantly higher quantitative CIS ratio for the DLB patients compared to the AD patients and controls (Table 2). The visual CIS scale had a similar diagnostic accuracy compared to the quantitative CIS ratio in distinguishing DLB patients from AD patients, but from a clinical perspective a visual rating scale is advantageous compared to a quantitative method for several reasons. A quantitative method can be time consuming, the actual value depends on both the acquisition and processing of the 18F-FDG-PET and MRI, and the specific software used may only be accessible in expert centres. A cut-off value may thus only be applicable to a specific setup in a single centre. In contrast, a visual rating scale for CIS can be implemented as a fast-diagnostic adjunct to the standard visual 18F-FDG-PET scan evaluation without additional software.

The visual CIS scale was also compared to another relevant 18F-FDG-PET feature (occipital hypometabolism) and to an overall visual evaluation of the 18F-FDG-PET image including typical and atypical features of DLB and AD (forced diagnosis). The performance for these 18F-FDG-PET visual features in distinguishing DLB from AD were consistent with two previous studies of similar ratings [21,31], and comparable to the visual CIS scale. This suggests that the visual CIS scale may supplement or even replace more resource demanding techniques performed by experienced nuclear medicine physicians.

Finally, we examined if the presence of CIS was influenced by concurrent Aβ pathology in DLB patients. Comparable to previous studies [7,20], we found that nearly half (46%) of the patient with a clinical diagnosis of DLB had an abnormal Aβ biomarker (Aβ+). Two previous studies consisting of a smaller study of 10 DLB patients [17]

and a larger study of 39 DLB patients [11] with determination of the brain Aβ status by 11C-PiB-PET found no association between a quantitative method of CIS and Aβ accumulation. Likewise, we found no significant differences between the DLB Aβ− patients and DLB Aβ+ patients for the quantitative CIS ratio. However, we found that the DLB Aβ− patients had the highest score on the visual CIS scale in comparison to the DLB Aβ+ patients with intermediate values (Table 2) as an indication of coexisting Aβ pathology may diminish the presence of CIS, although the difference only reached a trend level of $p = .06$.

Additionally, a cut-off visual CIS score of 4 discriminated the DLB Aβ− patients from DLB Aβ+ patients with a balanced accuracy of 70%, and this finding corroborate that Aβ pathology might be a possible confounding factor associated with the presence of CIS in DLB patients, which is relevant to include in the interpretation of CIS.

In general, the visual CIS scale distinguishes the diagnostic groups (DLB and AD) and the subgroups (DLB Aβ−, DLB Aβ+, and AD) with high specificities, but only moderate sensitivities. This may be explained by various potentially confounding circumstances. Previous studies have suggested that CIS may be influenced by the severity of cognitive impairment [11,30], however, in line with a previous study [15], we did not find a relationship between CIS and MMSE. The implementation of the visual CIS scale in a routine practice is potentially valuable considering that visual features including cingulate hypometabolism seemed to be underreported and missed on the clinical interpretation of FDG-PET scans of patients with DLB [13].

Combining the visual CIS scale on 18F-FDG-PET with visual assessment of atrophy pattern on MRI [32] could potentially increase the accuracy of DLB diagnosis and could be explored in future studies. Furthermore, the visual CIS scale should preferably be evaluated in a larger mixed memory cohort with unknown diagnosis and by less experienced readers.

Some limitations should be considered. In this study, the diagnosis of DLB and AD lacked pathological confirmation, but the reference diagnosis was based on reconfirmed diagnosis by an experienced dementia specialist (SGH, AH, and PH) according to the current DLB diagnostic criteria [25] and AD research criteria [27], and based on all available data including clinical follow up for at least 12 months for the majority of the patients.

Another limitation is the selection criteria, considering that we only included DLB patients with an Aβ biomarker and a 123I-FP-CIT-DAT-SPECT and AD patients with an Aβ biomarker, respectively, which are considered as supplementary disease biomarkers if the diagnosis is questionable in our clinics. Consequently, our study population may consist of patients with a more heterogenous clinical presentation, which may diminish the diagnostic accuracy. A final limitation is the use of different scanners given that the diagnostic workup for the study population was performed across several centres. On the other hand, visual ratings are in general more robust for scanner differences and should be applicable without consideration of the scanner.

Among the strengths of this study is the relatively large sample size with a comprehensive diagnostic evaluation program together with explicitly including DLB patients with an abnormal 123I-FP-CIT-DAT-SPECT. The latter is an indicative biomarker of DLB [26].

In conclusion, our study demonstrated that the visual CIS scale was robust and clinical applicable to evaluate the presence of CIS, which may help to improve the accuracy of clinical diagnosis of DLB. Furthermore, the degree of CIS may be associated with the presence of Aβ pathology in DLB patients. In perspective, the validity of the visual CIS scale should be evaluated in a larger mixed memory cohort and by less experienced readers.

Funding

This work was supported by the Rigshospitalet research board [R129-A5325].

Declaration of Competing Interest

All authors declare no conflicts of interest.

Acknowledgment

The authors wish to thank the Department of Clinical Physiology, Nuclear Medicine & PET, Rigshospitalet, Denmark, and in particular Oriol Puig Calvo for obtaining the 18F-FDG-PET scans of the healthy research volunteers, and Lisbeth Marner and Karine Madsen for valuable help with development of the visual CIS scale.

The authors wish to thank the Department of Neurology, Danish Dementia Research Centre, Rigshospitalet, Denmark, and in particular Asmus Vogel for assessing the neuropsychological tests of the healthy research volunteers.

Appendix A

A.1. Imaging details

A.1.1. MRI

MRI were acquired using a 1.5 Tesla GE Medical (Optima MR450w, Signa Hde, or Signa HDxt) ($n = 19$), 1.5 or 3 Tesla Philips (Achieva) ($n = 4$), or 1.5 or 3 Tesla Siemens (Aera, Avanto, Biograph, Espree, Trio, or Verio) ($n = 74$)

A.1.2. 123I-FP-CIT-DAT-SPECT

The DAT-SPECT imaging was performed according to the international practice guideline [5]. DAT-SPECT images were acquired using Triple-head IRIX camera (Philips Medical) ($n = 27$), PRISM 3000XP (Marconi, Philips) ($n = 5$), or Infina Hawkeye (GE) or Syngo Symbia T2 (Siemens) (n = 4)

In general, the SPECT image was acquired on either brain dedicated SPECT or general SPECT/CT systems 180–240 min after an intravenous bolus of 200 MBq 123I-FP-CIT.

A.1.3. 11C-PiB-PET

The PET imaging was performed according to the international practice guideline [28]. PET images were acquired using a Siemens Biograph mCT PET/CT scanner (Siemens Healthcare, Erlangen, Germany) ($n = 15$). In general, a 20–30 min static PET acquisition was performed on a standard PET/CT system 40 min after an intravenous bolus of 150–400 MBq 11C-PiB. After spatial normalization, images were analysed using clinical workstations, SyngoVia (SyngoVia, MI Neurology, Siemens Healthcare, Erlangen, Germany). The activity uptake in AD specific ROIs was defined [9], and uptake values calculated relative to cerebellar grey matter. The uptake was assessed after co-registration to the structural scan

A.1.4. 18F-FDG-PET

Imaging details are summarized in Table A.1

Table A.1
Imaging details for 18F-FDG-PET.

Subjects (n)	Scanner	Reconstruction method	Matrix size
2	GE Medical (Discovery MI)	QCFX or VPFXS	256 × 256
6	Philips (Gemini)	LOR-RAMLA or 3D-RAMLA	128 × 128
89	Siemens (Biograph mCT, Biograph mMR, or Somatom, 1094)	OSEM	336 × 336, 344 × 344, or 400 × 400

Abbreviations: n = numbers; 18F-FDG-PET = 18F-fluoro-deoxy-glucose positron emission tomography.

Appendix B

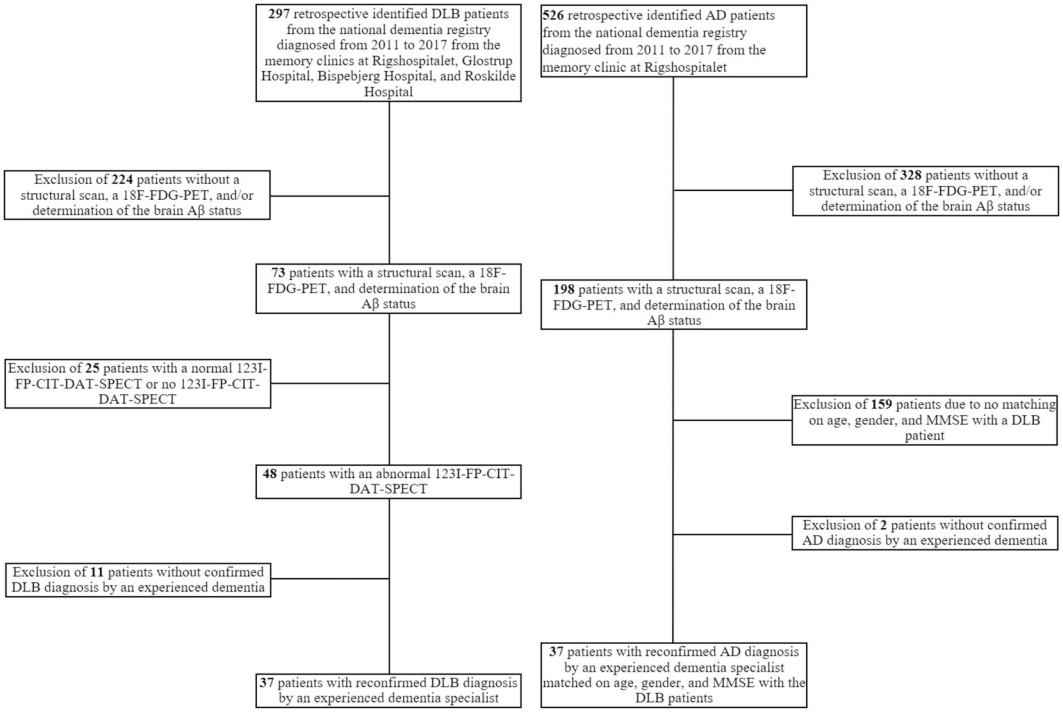

Fig. B.1. Flow diagram of the study population
Retrospective cohort study design and study flow diagram.

Appendix C

Table C.1
Distribution of the visual CIS scores between the two readers.

	Visual CIS score	Reader 1					Total
		0	1	2	3	4	
Reader 2	0	49	2	3	0	0	54
	1	5	3	2	0	1	11
	2	2	0	5	0	0	7
	3	0	3	4	0	3	10
	4	0	0	1	0	11	12
	Total	56	8	15	0	15	94

Abbreviations: CIS = cingulate island sign.

Appendix D

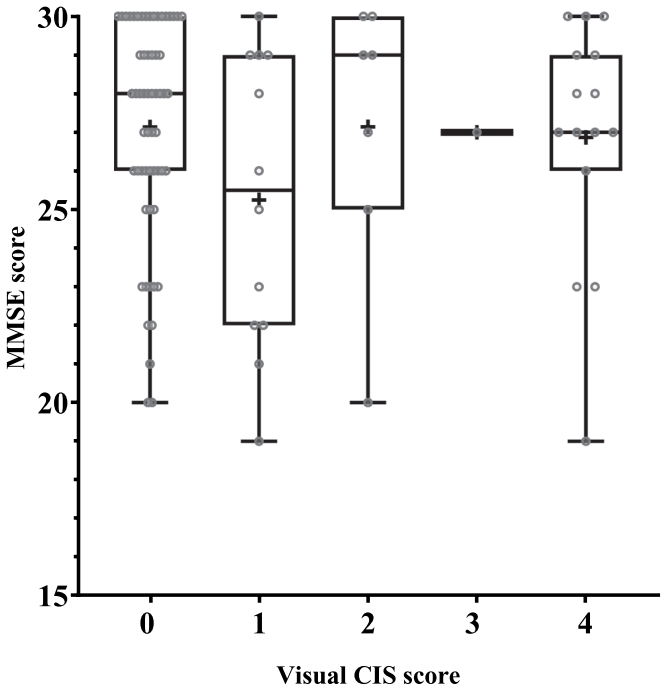

Fig. D.1. Boxplot for visual CIS score and MMSE score.
Abbreviations: CIS = cingulate island sign; MMSE = mini-mental state examination. Boxplot graph with the boxes corresponding to median values with indications of the 25th and 75th percentiles, and the whiskers show the minimum and maximum values. The + indicates the mean. All the subjects are plotted as ○. Overall comparison of all five groups on the visual CIS score (0, 1, 2, 3, and 4) and MMSE score with the Kruskal-Wallis tests (p = .55).

Table D.1
Correlation analysis between visual CIS score, MMSE score, age, education, and symptom duration for all subjects.

Correlation coefficient (r)	Visual CIS score	MMSE, score	Age, years	Education, years	Symptom duration, years
Visual CIS score	1.0	−0.08	−0.007	−0.11	0.12
MMSE, score	−0.08	1.0	−0.18	0.26*	−0.32*
Age, years	−0.007	−0.18	1.0	−0.06	−0.04
Education, years	−0.11	0.26*	−0.06	1.0	−0.26*

Abbreviations: CIS = cingulate island sign; FDG = false discovery rate; MMSE = Mini-Mental State Examination.
* $p < .05$ (FDR corrected).

Table D.2
Correlation analysis between visual CIS score, MMSE score, age, education, and symptom duration for DLB group.

Correlation coefficient (r)	Visual CIS score	MMSE, score	Age, years	Education, years	Symptom duration, years
Visual CIS score	1.0	0.21	0.02	0.13	−0.10
MMSE, score	0.21	1.0	−0.17	0.12	−0.02
Age, years	0.02	−0.17	1.0	−0.31	0.07
Education, years	0.13	0.12	−0.31	1.0	−0.15

Abbreviations: CIS = cingulate island sign; MMSE = Mini-Mental State Examination.

References

[1] R.L. Albin, S. Minoshima, C.J. D'Amato, K.A. Frey, D.A. Kuhl, A.A.F. Sima, Fluoro-deoxyglucose positron emission tomography in diffuse Lewy body disease, Neurology 47 (1996) 462–466.
[2] F.L. Andersen, C.N. Ladefoged, T. Beyer, S.H. Keller, A.E. Hansen, L. Højgaard, A. Kjær, I. Law, S. Holm, Combined PET/MR imaging in neurology: MR-based attenuation correction implies a strong spatial bias when ignoring bone, Neuroimage 84 (2014) 206–216. Available at https://doi.org/10.1016/j.neuroimage.2013.08.042.
[3] W.W. Barker, et al., Relative frequencies of Alzheimer disease, Lewy body, vascular and frontotemporal dementia, and hippocampal sclerosis in the State of Florida Brain Bank, Alzheimer Dis. Assoc. Disord. 16 (2002) 203–212.
[4] K.H. Brodersen, C.S. Ong, K.E. Stephan, J.M. Buhmann, The balanced accuracy and its posterior distribution. 2010, 20th Int Conf Pattern Recognit, 2010, pp. 3121–3124.
[5] J. Darcourt, J. Booij, K. Tatsch, A. Varrone, T.V. Borght, Ö. Kapucu, K. Någren, F. Nobili, Z. Walker, K. Van Laere, EANM procedure guidelines for brain neurotransmission SPECT using 123 I-labelled dopamine transporter ligands, version 2, Eur. J. Nucl. Med. Mol. Imaging 37 (2010) 443–450.
[6] P. Donaghy, A.J. Thomas, J.T. O'Brien, Amyloid PET imaging in Lewy body disorders, Am J Geriatr Psychiatry 23 (2015) 23–37. Available at https://doi.org/10.1016/j.jagp.2013.03.001.
[7] P. Edison, C.C. Rowe, J.O. Rinne, S. Ng, I. Ahmed, N. Kemppainen, V.L. Villemagne, G. O'Keefe, K. Någren, K.R. Chaudhury, C.L. Masters, D.J. Brooks, Amyloid load in

Parkinson's disease dementia and Lewy body dementia measured with [11C]PIB positron emission tomography, J. Neurol. Neurosurg. Psychiatry 79 (2008) 1331–1338.
[8] B. Fischl, FreeSurfer, Neuroimage 62 (2012) 774–781.
[9] A.S. Fleisher, K. Chen, X. Liu, A. Roontiva, P. Thiyyagura, N. Ayutyanont, A.D. Joshi, C.M. Clark, M.A. Mintun, M.J. Pontecorvo, P.M. Doraiswamy, K.A. Johnson, D.M. Skovronsky, E.M. Reiman, Using positron emission tomography and florbetapir F 18 to image cortical amyloid in patients with mild cognitive impairment or dementia due to Alzheimer disease, Arch. Neurol. 68 (2011) 1404–1411.
[10] H. Fujishiro, E. Iseki, S. Higashi, K. Kasanuki, N. Murayama, T. Togo, O. Katsuse, H. Uchikado, N. Aoki, K. Kosaka, H. Arai, K. Sato, Distribution of cerebral amyloid deposition and its relevance to clinical phenotype in Lewy body dementia, Neurosci Lett 486 (2010) 19–23. Available at https://doi.org/10.1016/j.neulet.2010.09.036.
[11] J. Graff-Radford, M.E. Murray, V.J. Lowe, B.F. Boeve, T.J. Ferman, S.A. Przybelski, T.G. Lesnick, M.L. Senjem, J.L. Gunter, G.E. Smith, D.S. Knopman, C.R. Jack Jr., D.W. Dickson, R.C. Petersen, K. Kejal, Dementia with Lewy bodies: basis of cingulate island sign, Neurology 83 (2014) 801–809.
[12] D.N. Greve, D.H. Salat, S.L. Bowen, D. Izquierdo-Garcia, A.P. Schultz, C. Catana, J.A. Becker, C. Svarer, G. Knudsen, R.A. Sperling, K.A. Johnson, Different partial volume correction methods lead to different conclusions: an 18 F-FDG-PET study of aging, Neuroimage 15 (2016) 334–343.
[13] M. Hamed, F. Schraml, J. Wilson, J. Galvin, M.N. Sabbagh, Occipital and cingulate hypometabolism are significantly under-reported on 18-Fluorodeoxyglucose positron emission tomography scans of patients with Lewy body dementia, J Alzheimers Dis Park 8 (2018) 1–12.
[14] P. Høgh, A.S. Teller, S. Hasselbalch, G. Waldemar, Visual rating and ROI-based parametric analysis of rCBF SPECT in patients with mild or questionable dementia: a comparative study, Dement. Geriatr. Cogn. Disord. 24 (2007) 429–433.
[15] T. Iizuka, M. Kameyama, Cingulate island sign on FDG-PET is associated with medial temporal lobe atrophy in dementia with Lewy bodies, Ann. Nucl. Med. 30 (2016) 421–429.
[16] D.J. Irwin, S.X. Xie, D. Coughlin, N. Nevler, R.S. Akhtar, C.T. McMillan, E.B. Lee, D.A. Wolk, D. Weintraub, A. Chen-Plotkin, J.E. Duda, M. Spindler, A. Siderowf, H.I. Hurtig, L.M. Shaw, M. Grossman, J.Q. Trojanowski, CSF-tau and β-amyloid predict cerebral synucleinopathy in autopsied Lewy body disorders, Neurology 90 (2018) 1038–1046.
[17] K. Ishii, C. Hosokawa, T. Hyodo, K. Sakaguchi, K. Usami, K. Shimamoto, M. Hosono, Y. Yamazoe, T. Murakami, Regional glucose metabolic reduction in dementia with Lewy bodies is independent of amyloid deposition, Ann. Nucl. Med. 29 (2015) 78–83.
[18] K. Ishii, T. Imamura, M. Sasaki, S. Yamaji, S. Sakamoto, H. Kitagaki, M. Hashimoto, N. Hirono, T. Shimomura, E. Mori, Regional cerebral glucose metabolism in dementia with Lewy bodies and Alzheimer's disease, Neurology 51 (1998) 125–130.
[19] K. Kantarci, V.J. Lowe, B.F. Boeve, S.D. Weigand, M.L. Senjem, S.A. Przybelski, D.W. Dickson, J.E. Parisi, D.S. Knopman, G.E. Smith, T.J. Ferman, R.C. Petersen, C.R. Jack Jr., Multimodality imaging characteristics of dementia with Lewy bodies, Neurobiol. Aging 33 (2012) 2091–2105.
[20] K. Kantarci, C. Yang, J.A. Schneider, M.L. Senjem, D.A. Reyes, V.J. Lowe, L.L. Barnes, N.T. Aggarwal, D.A. Bennett, G.E. Smith, R.C. Petersen, C.R. Jack Jr., B.F. Boeve, Ante mortem amyloid imaging and β-amyloid pathology in a case with dementia with Lewy bodies, Neurobiol Aging 33 (2012) 878–885. Available at https://doi.org/10.1016/j.neurobiolaging.2010.08.007.
[21] S.M. Lim, A. Katsifis, V.L. Villemagne, R. Best, G. Jones, M. Saling, J. Bradshaw, J. Merory, M. Woodward, M. Hopwood, C.C. Rowe, The 18F-FDG PET Cingulate Island sign and comparison to 123I-b-CIT SPECT for diagnosis of dementia with Lewy bodies, J. Nucl. Med. 50 (2009) 1638–1645.
[22] J. McCleery, S. Morgan, K.M. Bradley, A.H. Noel-Storr, O. Ansorge, C. Hyde, Dopamine transporter imaging for the diagnosis of dementia with Lewy bodies, Cochrane Database Syst. Rev. (2015) 1.
[23] I. McKeith, J.-P. Taylor, A. Thomas, P. Donaghy, J. Kane, Revisiting DLB diagnosis: a consideration of prodromal DLB and of the diagnostic overlap with Alzheimer disease, J. Geriatr. Psychiatry Neurol. 29 (2016) 249–253. Available at https://doi.org/10.1177/0891988716656083.
[24] I.G. McKeith, et al., Consensus guidelines for the clinical and pathologic diagnosis of dementia with Lewy bodies (DLB): report of the consortium on DLB international workshop, Neurology 47 (1996) 1113–1124.
[25] I.G. McKeith, et al., Diagnosis and management of dementia with Lewy bodies: third report of the DLB consortium, Neurology 65 (2005) 1863–1872.
[26] I.G. McKeith, et al., Diagnosis and management of dementia with Lewy bodies fourth consensus report of the DLB consortium, Neurology 89 (2017) 1–13.
[27] G.M. McKhann, D.S. Knopman, H. Chertkow, B.T. Hyman, C.R. Jack Jr., C.H. Kawas, W.E. Klunk, W.J. Koroshetz, J.J. Manly, R. Mayeux, R.C. Mohs, J.C. Morris, M.N. Rossor, P. Scheltens, M.C. Carrillo, B. Thies, S. Weintraub, C.H. Phelps, The diagnosis of dementia due to Alzheimer's disease: Recommendations from the National Institute on Aging-Alzheimer's Association workgroups on diagnostic guidelines for Alzheimer's disease, Alzheimer's Dement 7 (2011) 263–269. Available at: https://doi.org/10.1016/j.jalz.2011.03.005.
[28] S. Minoshima, A.E. Drzezga, H. Barthel, N. Bohnen, M. Djekidel, D.H. Lewis, C.A. Mathis, J. McConathy, A. Nordberg, O. Sabri, J.P. Seibyl, M.K. Stokes, K. Van Laere, SNMMI procedure standard/EANM practice guideline for amyloid PET imaging of the brain 1.0, J. Nucl. Med. 57 (2016) 1316–1322.
[29] S. Minoshima, N.L. Foster, A.A.F. Sima, K.A. Frey, R.L. Albin, D.E. Kuhl, Alzheimer's disease versus dementia with Lewy bodies: cerebral metabolic distinction with autopsy confirmation, Ann. Neurol. 50 (2001) 358–365.
[30] S. Morbelli, et al., Metabolic patterns across core features in dementia with Lewy bodies, Ann. Neurol. 85 (2019) 715–725.
[31] J.T. O'Brien, M.J. Firbank, C. Davison, N. Barnett, C. Bamford, C. Donaldson, K. Olsen, K. Herholz, D. Williams, J. Lloyd, 18F-FDG PET and perfusion SPECT in the diagnosis of Alzheimer and Lewy body dementias, J. Nucl. Med. 55 (2014) 1959–1965. Available at http://www.ncbi.nlm.nih.gov/pubmed/25453043.
[32] K. Oppedal, et al., A signature pattern of cortical atrophy in dementia with Lewy bodies: a study on 333 patients from the European DLB consortium, Alzheimers Dement. 15 (2019) 400–409.
[33] J.A. Schneider, Z. Arvanitakis, W. Bang, D.A. Bennett, Mixed brain pathologies account for most dementia cases in community-dwelling older persons, Neurology 69 (2007) 2197–2204.
[34] I. van Steenoven, D. Aarsland, D. Weintraub, E. Londos, F. Blanc, W.M. van der Flier, C.E. Teunissen, B. Mollenhauer, T. Fladby, M.G. Kramberger, L. Bonanni, A.W. Lemstra, Cerebrospinal fluid Alzheimer's disease biomarkers across the spectrum of Lewy body diseases: results from a large multicenter cohort, J. Alzheimers Dis. 54 (2016) 287–295.
[35] A. Varrone, S. Asenbaum, T.V. Borght, J. Booij, F. Nobili, K. Någren, J. Darcourt, Ö. Kapucu, K. Tatsch, P. Bartenstein, K. Van Laere, EANM procedure guidelines for PET brain imaging using [18F]FDG, version 2, Eur. J. Nucl. Med. Mol. Imaging 36 (2009) 2103–2110.
[36] M.W. Vernooij, F.B. Pizzini, R. Schmidt, M. Smits, T.A. Yousry, N. Bargallo, G.B. Frisoni, S. Haller, F. Barkhof, Dementia imaging in clinical practice: a European-wide survey of 193 centres and conclusions by the ESNR working group, Neuroradiology 61 (2019) 633–642.
[37] L.-O. Wahlund, E. Westman, D. van Westen, A. Wallin, S. Shams, L. Cavallin, E.-M. Larsson, Imaging biomarkers of dementia: recommended visual rating scales with teaching cases, Insights Imaging 8 (2017) 79–90. Available at https://doi.org/10.1007/s13244-016-0521-6.
[38] J.L. Whitwell, J. Graff-Radford, T.D. Singh, D.A. Drubach, M.L. Senjem, A.J. Spychalla, N. Tosakulwong, V.J. Lowe, K.A. Josephs, 18 F-FDG PET in posterior cortical atrophy and dementia with Lewy bodies, J. Nucl. Med. 58 (2017) 632–638. Available at https://doi.org/10.2967/jnumed.116.179903.
[39] W.J. Youden, Index for rating diagnostic tests, Cancer 3 (1950) 32–35.
[40] M.D. Zwan, J.O. Rinne, S.G. Hasselbalch, A. Nordberg, A. Lleó, S.-K. Herukka, H. Soininen, I. Law, J.M.C. Bahl, S.F. Carter, J. Fortea, R. Blesa, C.E. Teunissen, F.H. Bouwman, B.N.M. Van Berckel, P.J. Visser, Use of amyloid-PET to determine cutpoints for CSF markers, Neurology 86 (2016) 50–58.